

Joint Active And Passive IRS Aided Wireless Communication: Elements Allocation and Achievable Rate

Chaoying Huang, Wen Chen, *Senior Member, IEEE*, and Qingqing Wu, *Senior Member, IEEE*

Abstract—Equipping reflecting elements at the active intelligent reflecting surface (AIRS) enhances signal amplification capability but meanwhile incurs non-negligible amplification noise, which thus challenges the determination of elements allocation for maximizing achievable rate in multi-cooperative AIRS and passive IRS (PIRS) jointly aided wireless communication system. To tackle this issue, we consider the downlink communication from a single-antenna transmitter (Tx) to a single-antenna receiver (Rx), which is aided by a pair of AIRS and PIRS with two different deployment orders. Specifically, we target to determine the number of AIRS/PIRS elements over both transmission orders under given deployment budget for the achievable rate maximization. Our analysis illustrates that the PIRS should be allocated more elements than the AIRS for achieving optimized rate and linear signal-to-noise ratio (SNR) scaling orders are attained in both schemes. Simulation results are provided to evaluate the proposed algorithm and compare the rate performance of the AIRS and PIRS jointly aided wireless system with various benchmark systems.

Index Terms—Intelligent reflecting surfaces (IRS), active IRS, double IRSs, IRS elements allocation, rate maximization.

I. INTRODUCTION

Intelligent reflecting surface (IRS) has emerged as a promising technology to reconfigure the wireless radio propagation environment via smart signal reflections [1], [2]. Different from the conventional active relays, passive IRS (PIRS) is a low-cost meta-surface operating in the full-duplex mode with only passive signal reflection [3]. In particular, [4] leveraged PIRS to improve the physical layer security of an integrated sensing and communication (ISAC) system, while the active sensors were mounted at PIRS so-called semi-passive IRS for target localization in [5]. Additionally, [6] proposed a unified dynamic PIRS framework for achieving coverage extension with binary offloading. However, the conventional PIRS still remains a challenging issue that it practically suffers severe product-distance path loss resulting in radical limitation of power of multi-reflection signals [7].

Recently, the active IRS (AIRS) has proposed to efficiently compensate this PIRS issue by enabling simultaneous signal reflection and amplification which lead to a appreciable amplification power gain [8]. Note that since the AIRS equipped with massive active elements manipulated by reflection-type amplifiers, it non-negligibly incurs amplification noise in their reflected signals [7]. In particular, a received SNR scaling of $\mathcal{O}(M)$ with M reflecting active elements for the AIRS aided wireless system was proposed by [9], which is lower than double-PIRS case (i.e., $\mathcal{O}(M^4)$) where two cooperative PIRSs satisfied the optimal elements allocation of equal number [10],

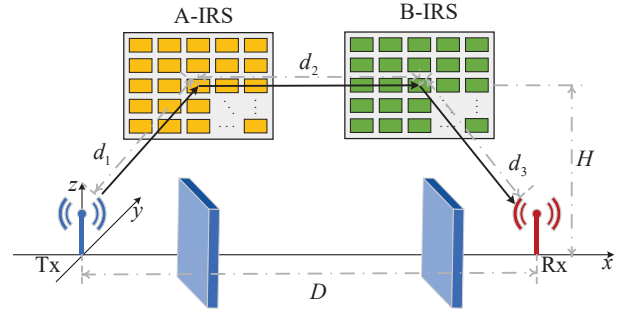


Fig. 1. The A-IRS and B-IRS jointly aided wireless communication system.

while the single AIRS outperforms the single PIRS in terms of rate when amplification power is high or M is small [9]. As it is beneficial to divide one single IRS into multiple smaller-size IRSs [3], [11] proposed a double-AIRS system with dynamic elements allocation yielding higher rate when M is moderate as compared to the single AIRS case. Furthermore, the joint employment of cooperative AIRS and PIRS was investigated in [12], which showed that the considerable performance gain achieved by the jointly optimized AIRS/PIRS deployment location over the double-PIRS and double-AIRS cases under the same power and IRS element budgets. In addition to deployment location, the elements allocation is also a significant role in cascaded multiple IRSs system under given deployment budget, which determines the power of reflected signal and coverage over each IRS. However, to the authors' best knowledge, the element allocation on a pair of cooperative AIRS and PIRS has not been studied yet.

To this end, we consider a double-IRS aided wireless communication system, where a pair of AIRS and PIRS are deployed as two transmission schemes, i.e., $\text{Tx} \rightarrow \text{AIRS} \rightarrow \text{PIRS} \rightarrow \text{Rx}$ (TAPR) and $\text{Tx} \rightarrow \text{PIRS} \rightarrow \text{AIRS} \rightarrow \text{Rx}$ (TPAR) schemes. Specifically, we target to determine the number of AIRS/PIRS elements over both transmission schemes under given deployment budget respectively for the achievable rate maximization. Our analysis illustrates that the PIRS should be allocated more elements than the AIRS for achieving optimized rate in both schemes. Besides, the TAPR outperforms TPAR in terms of achievable rate when the distance between the second IRS and Rx is sufficiently small or the AIRS amplification power is adequately large. Moreover, we show that the considered double-IRS aided systems attain linear SNR scaling orders, while both of schemes can achieve superior rate performance over various benchmarks.

II. SYSTEM MODEL AND PROBLEM FORMULATION

As illustrated in Fig.1, we consider a double-IRS aided wireless communication system, where active or passive IRS with proper elements jointly assist the communication from

C. Huang, W. Chen, and Q. Wu are with the Department of Electronic Engineering, Shanghai Jiao Tong University, Shanghai 200240, China (e-mail: chaoyinghuang@sjtu.edu.cn; wenchen@sjtu.edu.cn; qingqingwu@sjtu.edu.cn).

a single-antenna TX to a single-antenna Rx. Without loss of generality, we assume that the first IRS and the second IRS are expressed as A-IRS and B-IRS, respectively. Consider a three-dimensional (3D) Cartesian coordinate system, where the Tx, Rx, and two IRSs are located at $u_T = (0, 0, 0)$, $u_R = (D, 0, 0)$, $u_A = (x_A, 0, H)$ and $u_B = (x_B, 0, H)$, respectively. Assuming that the direct Tx-Rx link is blocked by arbitrary obstacles so that the data transmitting only via a double-reflection link over three line-of-sight (LOS) channel.

We denote that the two cascaded IRSs is equipped with N_A and N_B reflecting elements, respectively. Specifically, we define $\Psi_A = \text{diag}(\alpha_1 e^{j\varphi_1}, \dots, \alpha_{N_A} e^{j\varphi_{N_A}})$ and $\Phi_B = \text{diag}(\beta_1 e^{j\phi_1}, \dots, \beta_{N_B} e^{j\phi_{N_B}})$ as the reflection matrix of A-IRS and B-IRS respectively, where α_n/β_n and φ_n/ϕ_n correspondingly denote reflection amplitude and the phase shift. Furthermore, we set the common reflection amplitude factor of A-IRS and B-IRS elements as $\alpha_n = \alpha \geq 1, \forall n \in \mathcal{N}_A \triangleq \{1, \dots, N_A\}$ and $\beta_n = \beta \geq 1, \forall n \in \mathcal{N}_B \triangleq \{1, \dots, N_B\}$, separately, as the transmission signal arriving at each IRS experiences the same path loss under LOS channels. Moreover, let M represents the total deployment budget for the double-IRS with W_A and W_B respectively denoting the deployment cost of A-IRS and B-IRS elements.

Denote the distance between Tx and A-IRS as d_1 , the distance between A-IRS and B-IRS as d_2 , and the distance between B-IRS and Rx as d_3 . For ease of analysis, we assume the perfect channel state information (CSI) is to be known. Let $\mathbf{g}_{TA} \in \mathbb{C}^{N_A \times 1}$, $\mathbf{S}_{AB} \in \mathbb{C}^{N_B \times N_A}$, and $\mathbf{h}_{RB} \in \mathbb{C}^{N_B \times 1}$ represent the equivalent baseband LOS channel from the Tx to A-IRS, from the A-IRS to B-IRS, and from the B-IRS to Rx, respectively. Further, the Tx→A-IRS link is expressed as $\mathbf{g}_{TA} = \sqrt{\rho}/d_1 e^{-\frac{j2\pi d_1}{\lambda}} \mathbf{u}_{TA}(\theta_{TA}, \vartheta_{TA}, N_A)$, where $\mathbf{u}_{TA}(\theta_{TA}, \vartheta_{TA}, N_A) = \mathbf{a}(\frac{2d_1}{\lambda} \sin(\theta_{TA}) \sin(\vartheta_{TA}), N_{A,x}) \otimes \mathbf{a}(\frac{2d_1}{\lambda} \cos(\vartheta_{TA}), N_{A,y})$, $N_A = N_{A,x} \times N_{A,y}$ and $\mathbf{a}(w, N) = [1, \dots, e^{-j\pi(N-1)w}]^T$. $(\theta_{TA}, \vartheta_{TA}) \in [0, \pi]$, λ , and ρ denote the angle-of-arrival pair, the wavelength and the channel power gain at the reference distance of 1m, respectively. Similarly, the A-IRS→B-IRS link is given by $\mathbf{S}_{AB} = \sqrt{\rho}/d_2 e^{-\frac{j2\pi d_2}{\lambda}} \mathbf{u}_{AB}(\theta_{AB}, \vartheta_{AB}, N_B) \mathbf{u}_{BA}^H(\theta_{BA}, \vartheta_{BA}, N_A)$, and the B-IRS→Rx link is given by $\mathbf{h}_{RB} = \sqrt{\rho}/d_3 e^{-\frac{j2\pi d_3}{\lambda}} \mathbf{u}_{RB}(\theta_{RB}, \vartheta_{RB}, N_B)$.

We maximize the achievable rate R among Rx of the above TAPR and TPAR transmission schemes by optimizing the elements allocation of A-IRS and B-IRS, $\{N_A, N_B\}$ and the reflection matrices of A-IRS and B-IRS, $\{\Psi_A, \Phi_B\}$. Given N_A and N_B , the optimal phase shifts of double-IRS are expressed as [12]

$$\varphi_n = \arg([\mathbf{u}_{BA}]_n) - \arg([\mathbf{u}_{TA}]_n), \forall n \in \mathcal{N}_A, \quad (1)$$

$$\phi_n = \arg([\mathbf{u}_{AB}]_n) - \arg([\mathbf{u}_{RB}]_n), \forall n \in \mathcal{N}_B. \quad (2)$$

As such, our objective is reduced to maximize the achievable rate by jointly optimizing the number of A-IRS and B-IRS elements, $\{N_A, N_B\}$, and the reflection amplitude factors of A-IRS and B-IRS, $\{\alpha, \beta\}$, for the TAPR and TPAR schemes under the limited total elements budget, which would be discuss in detail as following.

A. TAPR Transmission Scheme

We first consider the TAPR deployment scheme with $N_A = N_{\text{act}}$, $N_B = N_{\text{pas}}$, $W_A = W_{\text{act}}$ and $W_B = W_{\text{pas}}$, where N_{act} and N_{pas} denote the number of the AIRS and PIRS elements respectively. W_{act} represents the deployment cost of each active element, which is larger than that of each passive element W_{pas} as its more sophisticated hardware and higher static operation power. Since the A-IRS is active and B-IRS is passive in the TAPR system, we further set the reflection amplitude factor of A-IRS as $\beta = 1$ and that of B-IRS still constrain to $\alpha \geq 1$.

1) *System Model*: According to the deployment strategy of TAPR scheme with Tx → AIRS → PIRS → Rx transmission link, the signal received at the Rx is obtained as

$$y_{AP} = \mathbf{h}_{RP}^H \Phi_{\text{pas}} \mathbf{S}_{AP} \Psi_{\text{act}} \mathbf{g}_{TA} s + \mathbf{h}_{RP}^H \Phi_{\text{pas}} \mathbf{S}_{AP} \Psi_{\text{act}} \mathbf{v} + n_0, \quad (3)$$

where s denotes the transmitted signal for Rx with power P_t , $\mathbf{v} \in \mathbb{C}^{N_{\text{act}} \times 1}$ is the amplification noise introduced by active elements of AIRS satisfying the independent circularly symmetric complex Gaussian (CSCG) distribution $\mathbf{v} \sim \mathcal{CN}(\mathbf{0}_{N_{\text{act}}}, \sigma_v^2 \mathbf{I}_{N_{\text{act}}})$ with the amplification noise power σ_v , and $n_0 \sim \mathcal{CN}(0, \sigma_0^2)$ is the additive white Gaussian noise (AWGN) at the Rx. The corresponding received signal-to-noise ratio (SNR) of the receiver is given by

$$\gamma_{AP} = \frac{P_t \left| \mathbf{h}_{RP}^H \Phi_{\text{pas}} \mathbf{S}_{AP} \Psi_{\text{act}} \mathbf{g}_{TA} \right|^2}{\sigma_v^2 \left\| \mathbf{h}_{RP}^H \Phi_{\text{pas}} \mathbf{S}_{AP} \Psi_{\text{act}} \right\|^2 + \sigma_0^2}. \quad (4)$$

Therefore, the achievable rate in bits per second per Hertz (bps/Hz) for the TAPR transmission system is

$$R_{AP} = \log_2(1 + \gamma_{AP}). \quad (5)$$

2) *Problem Formulation*: We aim to maximize the achievable rate for the Rx by jointly optimizing the elements allocation of the AIRS and PIRS $\{N_{\text{act}}, N_{\text{pas}}\}$ and the reflection amplitude factor of the AIRS $\{\alpha\}$ for the TAPR scheme, which is formulated as follows.

$$\begin{aligned} \text{(P1)} \quad & \underset{N_{\text{act}}, N_{\text{pas}}, \alpha}{\text{maximize}} && R_{AP} \\ & \text{s.t.} && W_{\text{act}} N_{\text{act}} + W_{\text{pas}} N_{\text{pas}} \leq M, \quad (6) \\ & && P_t \|\Psi_{\text{act}} \mathbf{g}_{TA}\|^2 + \sigma_v^2 \|\Psi_{\text{act}}\|^2 \leq P_v, \quad (7) \\ & && \alpha \geq 1, \quad (8) \\ & && N_{\text{act}} > 0, \quad (9) \\ & && N_{\text{pas}} > 0, \quad (10) \end{aligned}$$

where P_v denotes the given amplification power budget of all AIRS elements. Since the objective function is increasing with the amplification power factor α , the equality in constraint (7) always holds at the optimal solution of problem (P1). It is not difficult to verify that the optimal amplification factor with given $\{N_{\text{act}}, N_{\text{pas}}\}$ satisfies $\alpha^* = \sqrt{P_v d_1^2 / (P_t \rho N_{\text{act}} + d_1^2 \sigma_v^2 N_{\text{act}})}$. Hence, the received SNR can be further expressed as $\gamma_{AP} = P_t P_v \rho^3 / \zeta_{AP}$, where

$$\zeta_{AP} = \frac{P_v \sigma_v^2 \rho^2 d_1^2}{N_{\text{act}}} + \frac{\sigma_0^2 d_2^2 d_3^2 (\rho P_t + \sigma_v^2 d_1^2)}{N_{\text{act}} N_{\text{pas}}^2}. \quad (11)$$

Based on the above discussion, problem (P1) can be equivalent to the following problem (P2).

$$(P2) \quad \underset{N_{\text{act}}, N_{\text{pas}}}{\text{minimize}} \quad \zeta_{\text{AP}} \\ \text{s.t.} \quad \text{Constraints (6), (9), (10).} \quad (12)$$

It is challenge to solve (P2) due to the integer constrains (9), (10) and the non-convex objective function. To tackle this difficulty, we first relax the integer values $\{N_{\text{act}}, N_{\text{pas}}\}$ into the continuous values $\{x_{\text{act}}, x_{\text{pas}}\}$. Then, we introduce the slack variables $\tilde{x}_a = \log(x_{\text{act}})$ and $\tilde{x}_p = \log(x_{\text{pas}})$, yielding the objective function transform to

$$\tilde{\zeta}_{\text{AP}} = C_1^{\text{AP}} e^{-\tilde{x}_a} + (C_2^{\text{AP}} + C_3^{\text{AP}}) e^{-\tilde{x}_a - 2\tilde{x}_p}, \quad (13)$$

where $C_1^{\text{AP}} = P_v \sigma_v^2 \rho^2 d_1^2$, $C_2^{\text{AP}} = \sigma_0^2 d_2^2 d_3^2 \rho P_t$, and $C_3^{\text{AP}} = \sigma_0^2 \sigma_v^2 d_1^2 d_2^2 d_3^2$. Thus, (P2) is correspondingly expressed as

$$(P2.1) \quad \underset{\tilde{x}_a, \tilde{x}_p}{\text{minimize}} \quad \tilde{\zeta}_{\text{AP}} \\ \text{s.t.} \quad W_{\text{act}} e^{\tilde{x}_a} + W_{\text{pas}} e^{\tilde{x}_p} \leq M. \quad (14)$$

It is not difficult to derive that the constrain (14) needs to be active for the optimal solution of (P2.1). Thus, we can demonstrate that (P2.1) is a convex optimization problem as its convex objective function and constrain, which can be optimally solved by existing convex optimization solvers such as CVX. By rounding the optimal continuous solutions, the integer elements allocation of AIRS and PIRS can be reconfigured.

Proposition 1. *Given the optimal reflection matrix of the cooperative double-IRS, the achievable rate for TAPR with M as $M \rightarrow \infty$ according to*

$$\lim_{M \rightarrow \infty} \frac{R_{\text{AP}}}{\log_2 M} = 1. \quad (15)$$

Proof: Assume $N_{\text{act}} = rM$ and $N_{\text{pas}} = (1-r)M$ with $0 < r < 1$. As $M \rightarrow \infty$, it holds that

$$\lim_{M \rightarrow \infty} \zeta_{\text{AP}} = \lim_{M \rightarrow \infty} \frac{P_v \sigma_v^2 \rho^2 d_1^2}{rM} + \frac{\sigma_0^2 d_2^2 d_3^2 (\rho P_t + \sigma_v^2 d_1^2)}{r(1-r)^2 M^3} \\ = \lim_{M \rightarrow \infty} \frac{P_v \sigma_v^2 \rho^2 d_1^2}{rM} + o\left(\frac{1}{M}\right). \quad (16)$$

Accordingly, we have $\lim_{M \rightarrow \infty} \frac{R_{\text{AP}}}{\log_2 M} = 1$. Note that as the received signal attains the multiplicative beamforming gain through double-reflection, its power subsequently increases in the order of $\mathcal{O}(M^4)$ (see [10]). However, the noise power scales with the order of $\mathcal{O}(M^3)$ when $M \rightarrow \infty$ leading to the received SNR scaling order of $\mathcal{O}(M)$ for the TAPR system, which is lower than the double-passive-IRS case (i.e., $\mathcal{O}(M^4)$). ■

B. TPAR Transmission Scheme

Then, consider the TPAR scheme with $N_A = N_{\text{pas}}$, $N_B = N_{\text{act}}$, $W_A = W_{\text{pas}}$ and $W_B = W_{\text{act}}$. We set the amplification factors as $\alpha = 1$ and $\beta \geq 1$, since the A-IRS is passive and B-IRS is active in the TPAR transmission scheme. According to the placement order of the aforementioned two IRSs, the received signal at Rx for TPAR can be shown as

$$y_{\text{PA}} = \mathbf{h}_{\text{RA}}^H \Phi_{\text{act}} \mathbf{S}_{\text{PA}} \Psi_{\text{pas}} \mathbf{g}_{\text{TP}} s + \mathbf{h}_{\text{RA}}^H \Phi_{\text{act}} \mathbf{v} + n_0. \quad (17)$$

As such, the corresponding SNR at Rx is obtained as

$$\gamma_{\text{PA}} = \frac{P_t \left| \mathbf{h}_{\text{RA}}^H \Phi_{\text{act}} \mathbf{S}_{\text{PA}} \Psi_{\text{pas}} \mathbf{g}_{\text{TP}} \right|^2}{\sigma_v^2 \left\| \mathbf{h}_{\text{RA}}^H \Phi_{\text{act}} \right\|^2 + \sigma_0^2}. \quad (18)$$

Similar to the amplification power constrain in TAPR, the optimal amplification factor satisfies $\beta^* = \sqrt{P_v d_2^2 / (P_t \rho^2 x_a x_p^2 / d_1^2 + d_2^2 \sigma_v^2 x_a)}$. By substituting β^* to (18), we execute the SNR re-expression as $\gamma_{\text{PA}} = P_t P_v \rho^3 / \zeta_{\text{PA}}$, where

$$\zeta_{\text{PA}} = \frac{P_t \sigma_0^2 \rho^2 d_3^2}{x_a} + \frac{\sigma_v^2 d_1^2 d_2^2 (\rho P_v + \sigma_0^2 d_3^2)}{x_a x_p^2}. \quad (19)$$

By introducing the slack variables $\tilde{x}_a = \log(x_{\text{act}})$ and $\tilde{x}_p = \log(x_{\text{pas}})$ similarly to TAPR, the equality (19) can be re-shown as

$$\tilde{\zeta}_{\text{PA}} = (C_1^{\text{PA}} + C_2^{\text{PA}}) e^{-\tilde{x}_a - 2\tilde{x}_p} + C_3^{\text{PA}} e^{-\tilde{x}_a}, \quad (20)$$

where $C_1^{\text{PA}} = \sigma_v^2 d_1^2 d_2^2 \rho P_v$, $C_2^{\text{PA}} = \sigma_v^2 d_1^2 d_2^2 \sigma_0^2 d_3^2$, and $C_3^{\text{PA}} = P_t \sigma_0^2 \rho^2 d_3^2$. Thus, the optimization problem for TPAR is formulated as

$$(P3) \quad \underset{\tilde{x}_a, \tilde{x}_p}{\text{minimize}} \quad \tilde{\zeta}_{\text{PA}} \\ \text{s.t.} \quad W_{\text{act}} e^{\tilde{x}_a} + W_{\text{pas}} e^{\tilde{x}_p} \leq M. \quad (21)$$

It is not difficult to verify that the problem (P3) is convex, so that its optimal solution can be obtained by CVX tool.

Proposition 2. *Given the optimal reflection matrix of the cooperative double-IRS, the achievable rate for TPAR with M as $M \rightarrow \infty$ according to*

$$\lim_{M \rightarrow \infty} \frac{R_{\text{PA}}}{\log_2 M} = 1. \quad (22)$$

The proof is similar to that of Proposition 1, which is neglected for brevity.

III. LOW-COMPLEXITY ALLOCATION DESIGN AND PERFORMANCE ANALYSIS

In this section, we propose suboptimal solutions of elements allocation in closed-form for the TAPR and TPAR schemes, which are able to reduce computational complexity and shed meaningful insights.

A. Suboptimal Solutions

For simplifying (11) and (19), we first provide a helpful Lemma which the proof is ignored for brevity.

Lemma 1. *We have $(C_2^{\text{AP}} + C_3^{\text{AP}}) \gg C_1^{\text{AP}}$ and $C_1^{\text{PA}} \gg \max(C_2^{\text{PA}}, C_3^{\text{PA}})$, if*

$$\min\left(\frac{\sigma_0 d_2}{\sqrt{P_v \rho} x_{\text{pas}}}, \frac{\sigma_0}{\sqrt{P_v \rho}}, \frac{\sqrt{P_v} d_1 d_2 \sigma_v}{\sqrt{P_t \rho \sigma_0} x_{\text{pas}}}\right) \gg d_3 \quad (23)$$

1) *TAPR Scheme:* Based on Lemma 1, the achievable rate at the Rx for the TAPR can be approximated as $\bar{R}_{\text{AP}} = \log_2(1 + P_t P_v \rho^3 / \tilde{\zeta}_{\text{AP}}(x_{\text{act}}, x_{\text{pas}}))$, where $\tilde{\zeta}_{\text{AP}}(x_{\text{act}}, x_{\text{pas}}) =$

$\frac{\sigma_0^2 d_2^2 d_3^2 (\rho P_t + \sigma_v^2 d_1^2)}{x_{\text{act}} x_{\text{pas}}^2}$. Thus, the problem (P1) is expressed approximately as

$$(P5) \quad \min_{x_{\text{act}}, x_{\text{pas}}} \bar{\zeta}_{\text{AP}} \quad (24)$$

$$\text{s.t. } W_{\text{act}} x_{\text{act}} + W_{\text{pas}} x_{\text{pas}} \leq M \quad (24)$$

$$x_{\text{act}} > 0, \quad (25)$$

$$x_{\text{pas}} > 0. \quad (26)$$

The optimal solution to (P5) is shown as follows.

Lemma 2. *The optimal solution to (P5) is*

$$\bar{x}_{\text{act}}^* = \frac{M}{3W_{\text{act}}}, \quad \bar{x}_{\text{pas}}^* = \frac{2M}{3W_{\text{pas}}}. \quad (27)$$

Proof: Note that the constrain (24) always satisfies equality in the optimal solution since the objective function increases with M . We take the first-order derivative of $\bar{\zeta}_{\text{AP}}$ over x_{pas} with $x_{\text{act}} = \frac{M - W_{\text{pas}} x_{\text{pas}}}{W_{\text{act}}}$ as

$$\frac{d\bar{\zeta}_{\text{AP}}}{dx_{\text{pas}}} = \frac{-C_2^{\text{AP}} f_1(x_{\text{pas}})}{(M x_{\text{pas}}^2 - W_{\text{pas}} x_{\text{pas}}^3)^2}, \quad (28)$$

where $f_1(x_{\text{pas}}) = 2M x_{\text{pas}} - 3W_{\text{pas}} x_{\text{pas}}^2$. Note that $f_1(x_{\text{pas}})$ is a quadratic function. Meanwhile when $x_{\text{pas}} > 0$, we have $f_1(x_{\text{pas}}) > 0$, when $x_{\text{pas}} > M$, we have $f_1(x_{\text{pas}}) < 0$, there exists one and only one root of $f_1(x_{\text{pas}})$ within $(0, M)$, i.e., $x_{\text{pas}}^{\text{rt}} = \frac{2M}{3W_{\text{pas}}}$. Furthermore, when $0 < x_{\text{pas}} < x_{\text{pas}}^{\text{rt}}$, $\frac{d\bar{\zeta}_{\text{AP}}}{dx_{\text{pas}}} < 0$ holds, i.e., $\bar{\zeta}_{\text{AP}}$ monotonically decreases with x_{pas} . When $x_{\text{pas}}^{\text{rt}} < x_{\text{pas}} < M$, $\frac{d\bar{\zeta}_{\text{AP}}}{dx_{\text{pas}}} > 0$ holds, i.e., $\bar{\zeta}_{\text{AP}}$ monotonically increases with x_{pas} . Accordingly, $f_1(x_{\text{pas}})$ is minimized at $x_{\text{pas}}^* = x_{\text{pas}}^{\text{rt}}$, which completes the proof. ■

Proposition 3. *By suboptimally equipping AIRS and PIRS for a TAPR system with the condition (23), deploying two cooperative IRSs with optimal phase shift given in (1) and (2) result in M^3 -fold scaling order of the received SNR, i.e.,*

$$\bar{\gamma}_{\text{AP}} = \frac{4M^3 P_t P_v \rho^3}{27\sigma_0^2 d_2^2 d_3^2 (\rho P_t + \sigma_v^2 d_1^2) W_{\text{act}} W_{\text{pas}}^2} \quad (29)$$

Note that Proposition 3 is not difficult to proof by substituting (27) into the SNR for TAPR, which can be explained as follows. As the received signal experiences double-reflection which contribute to the multiplicative beamforming gain, its power subsequently increases in the order of $\mathcal{O}(M^4)$. While the noise power mainly scales with the order of $\mathcal{O}(M)$ when d_3 is considerable small, engendering the received SNR scaling order of $\mathcal{O}(M^3)$ for the TAPR system, which is higher than the scaling for the single-active-IRS case (i.e., $\mathcal{O}(M)$ [9]).

2) *TPAR Scheme:* Thanks to Lemma 1, the achievable rate for TPAR can be simplified to $\bar{R}_{\text{PA}} = \log_2(1 + P_t P_v \rho^3 / \bar{\zeta}_{\text{PA}}(x_{\text{act}}, x_{\text{pas}}))$, where $\bar{\zeta}_{\text{PA}}(x_{\text{act}}, x_{\text{pas}}) = \frac{d_1^2 d_2^2 \sigma_v^2 \rho P_v}{x_{\text{act}} x_{\text{pas}}^2}$, yielding (P3) rewrite as

$$(P6) \quad \min_{x_{\text{act}}, x_{\text{pas}}} \bar{\zeta}_{\text{PA}} \quad (30)$$

$$\text{s.t. Constrains (33), (34), (35). \quad (30)}$$

Lemma 3. *The optimal solution to (P6) is given by*

$$\bar{x}_{\text{act}}^* = \frac{M}{3W_{\text{act}}}, \quad \bar{x}_{\text{pas}}^* = \frac{2M}{3W_{\text{pas}}}. \quad (31)$$

The proof is similar to that of Lemma 2, which is neglected for brevity. It is interesting to note that the elements allocation to the AIRS and PIRS among the TAPR and TPAR schemes tends to be the same in the common deployment, while the PIRS are allocated more resources than the AIRS.

Proposition 4. *By suboptimally equipping PIRS and AIRS for a TPAR system with the condition (23), deploying two cooperative IRSs with optimal phase shift given in (1) and (2) result in M^3 -fold scaling order of the received SNR, i.e.,*

$$\bar{\gamma}_{\text{PA}} = \frac{4M^3 P_t \rho^3}{27d_1^2 d_2^2 \sigma_v^2 \rho W_{\text{act}} W_{\text{pas}}^2}. \quad (32)$$

Obviously, Proposition 2 can be proofed straightly by substituting (31) into the received SNR for TPAR.

B. TAPR Versus TPAR

Based on the suboptimal AIRS and PIRS elements allocation given in (27) and (31), we take the achievable rates of the TAPR and TPAR systems into comparison as follows.

Proposition 5. *The achievable rate of TAPR is no less than that of TPAR, i.e., $\bar{R}_{\text{AP}} \geq \bar{R}_{\text{PA}}$, when*

$$\frac{1}{\rho} \leq \frac{P_v}{d_3^2 \sigma_0^2} - \frac{P_t}{d_1^2 \sigma_v^2}, \quad (33)$$

with the condition in (23). Otherwise, $\bar{R}_{\text{AP}} < \bar{R}_{\text{PA}}$.

Proof: As the achievable rate monotonically increases with the SNR, it is feasible to compare $\bar{\zeta}_{\text{AP}}$ and $\bar{\zeta}_{\text{PA}}$ instead of \bar{R}_{AP} and \bar{R}_{PA} , i.e.,

$$\begin{aligned} \bar{\zeta}_{\text{AP}} - \bar{\zeta}_{\text{PA}} &= k \left(\frac{1}{\sigma_0^2 d_2^2 d_3^2 (\rho P_t + \sigma_v^2 d_1^2)} - \frac{1}{d_1^2 d_2^2 \sigma_v^2 \rho P_v} \right) \\ &= \frac{k \left(\frac{P_v}{d_3^2 \sigma_0^2} - \frac{P_t}{d_1^2 \sigma_v^2} - \frac{1}{\rho} \right)}{P_v d_2^2 (\rho P_t + \sigma_v^2 d_1^2)}, \end{aligned} \quad (34)$$

where $k = \frac{4M^3 P_t P_v \rho^3}{27W_{\text{act}} W_{\text{pas}}^2} > 0$. As such, we have $\bar{\zeta}_{\text{AP}} \geq \bar{\zeta}_{\text{PA}}$, i.e., $\bar{R}_{\text{AP}} \geq \bar{R}_{\text{PA}}$, when $\frac{1}{\rho} \leq \frac{P_v}{d_3^2 \sigma_0^2} - \frac{P_t}{d_1^2 \sigma_v^2}$, which completes the proof. Note that the condition in (33) can be practically satisfied when the AIRS amplification power is high or the distance d_3 is sufficiently small. ■

IV. SIMULATION RESULTS

In this section, numerical results are provided to compare the rate performance of the considered TAPR and TPAR transmission systems with other benchmarks. The deployment locations of the Tx, the A-IRS, the B-IRS and the Rx are set as (0,0,0), (8,0,2), (58,0,2) and (58,0,0) in meters (m), respectively. We set the carrier frequency as 5GHz and thus the channel power gain at the reference distance of 1m is $\rho = -40\text{dB}$. Other parameters are set as $P_t = 20\text{dBm}$, $P_v = 10\text{dBm}$, $\sigma_0^2 = \sigma_v^2 = -80\text{dBm}$, $W_{\text{act}} = 1.2$ and $W_{\text{pas}} = 1$. We consider other four systems as benchmarks that compare with the TAPR and TPAR systems, including a single PIRS, a single AIRS, a hybrid IRS, as well as double PIRSs. For the sake of fairness, we set the same transmit power and amplification power budget for different systems, while the transmit power is $(P_t + P_v)$ for the single PIRS and double PIRSs cases.

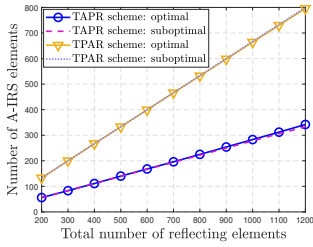


Fig. 2. Number of A-IRS elements versus total number of elements.

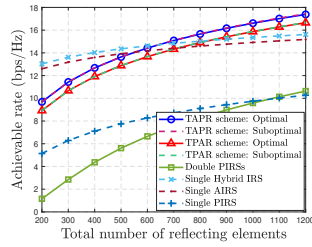


Fig. 3. Achievable rate versus total number of elements.

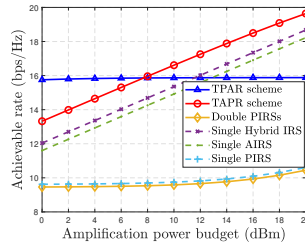


Fig. 4. Achievable rate versus amplification power of active elements.

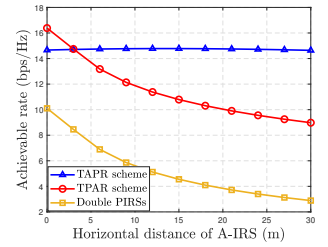


Fig. 5. Achievable rate versus horizontal distance of A-IRS.

In Fig. 1, we depict the number of A-IRS elements versus the total number of reflecting elements. It is observed that the proposed suboptimal solution yields near-optimal designs, verifying the effectiveness of Lemma 1. In addition, the number of A-IRS elements monotonically increases with the total number of elements while the PIRS is equipped more elements compared to AIRS in both schemes, which agree exceptionally well with Lemma 2 and Lemma 3.

Fig. 2 shows that the achievable rate of various systems versus total number of reflecting elements. Once again, our proposed suboptimal solution of elements allocation yields near-optimal performance in both TAPR and TPAR schemes in agreement with Lemma 1. Besides, the TAPR system outperforms the TPAR system when $\frac{1}{\rho} \leq \frac{P_v}{d_3^2 \sigma_0^2} - \frac{P_t}{d_1^2 \sigma_v^2}$, because it suffers less amplification noise power at the Rx and thus obtains better SNR. The result agrees exceptionally well with Proposition 5. Furthermore, the single AIRS and single hybrid IRS system achieves higher rate than the TAPR and TPAR cases when M is small. However, the TAPR and TPAR system yield the best rate performance with M constantly increasing because they provide considerable amplification power gain compared with other systems.

In Fig. 3, we compare the achievable rate with optimal elements allocation versus amplification power budget of active elements, a limited total number of reflecting elements of 1000 for different schemes. It can be observed that the rate performance of the TAPR system increases due to the growing amplification power, while that of the TPAR system keeps almost constant because the AIRS in the TPAR system is extremely close to the Rx leading to higher amplification noise power which balance the achievable rate up. Moreover, when P_v is small, the rate performance of TPAR exceeds that of TAPR and other benchmarks. Additionally, the achievable rate of TPAR is in line with the TAPR case when $P_v \approx 8\text{dBm}$. Lastly, when P_v is adequately large, the TAPR scheme achieve the best rate performance because it strikes a dynamical balance between signal and noise amplification. Fig. 4 clearly indicates that the AIRS in TPAR system need to be deployed closely to the Tx for higher achievable rate while the deployment placement of PIRS in TAPR system influences negligibly the rate performance as the AIRS is stationary, and both of the two schemes outperform the double PIRs case.

V. CONCLUSION

In this paper, we studied the elements allocation problem for maximizing the achievable rate with the total amplification

power and total reflecting elements in AIRS-PIRS jointly aided wireless communication system. By introducing the slack variables, we derived the optimal solution and characterized the SNR scaling orders for the TAPR and TPAR transmission schemes. To gain more useful insights, we provided the closed-form expressions for the near-optimal solution which revealed that TAPR outperforms TPAR in terms of achievable rate when d_3 is adequately small or the AIRS amplification power is sufficiently high, while the PIRS should be allocated more resources than the AIRS in both schemes. Numerical results were presented to validated our analysis and indicated that the wireless system aided by a pair of AIRS and PIRS we considered achieve higher rate performance than the existing benchmarks under the same power and element budgets when M is relatively large.

REFERENCES

- [1] Q. Wu, S. Zhang, B. Zheng, C. You, and R. Zhang, "Intelligent reflecting surface aided wireless communications: A tutorial," *IEEE Trans. Commun.*, vol. 69, no. 5, pp. 3313–3351, May 2021.
- [2] Q. Wu, X. Zhou, W. Chen, J. Li and X. Zhang, "IRS-aided WPCNs: A new optimization framework for dynamic IRS beamforming," *IEEE Trans. Wireless Commun.*, vol. 21, no. 7, pp. 4725–4739, Jul. 2022.
- [3] Z. Kang, C. You and R. Zhang, "IRS-aided wireless relaying: Deployment strategy and capacity scaling," *IEEE Wireless Commun. Lett.*, vol. 11, no. 2, pp. 215–219, Feb. 2022.
- [4] M. Hua, Q. Wu, W. Chen, O. A. Dobre and A. L. Swindlehurst, "Secure intelligent reflecting surface aided integrated sensing and communication," *IEEE Trans. Wireless Commun.*, Jun. 2023.
- [5] M. Hua, Q. Wu, W. Chen, Z. Fei, H. C. So and C. Yuen, "Intelligent reflecting surface-assisted localization: Performance analysis and algorithm design," *IEEE Wireless Commun. Lett.*, vol. 13, no. 1, pp. 84–88, Jan. 2024.
- [6] G. Chen, Q. Wu, R. Liu, J. Wu and C. Fang, "IRS aided MEC systems with binary offloading: A unified framework for dynamic IRS beamforming," *IEEE J. Sel. Areas Commun.*, vol. 41, no. 2, pp. 349–365, Feb. 2023.
- [7] R. Long, Y.-C. Liang, Y. Pei, and E. G. Larsson, "Active reconfigurable intelligent surface-aided wireless communications," *IEEE Trans. Wireless Commun.*, vol. 20, no. 8, pp. 4962–4975, Aug. 2021.
- [8] Y. Li, C. You, and Y. J. Chun, "Active-IRS aided wireless network: System modeling and performance analysis," *IEEE Commun. Lett.*, vol. 27, no. 2, pp. 487–491, Nov. 2023.
- [9] C. You and R. Zhang, "Wireless communication aided by intelligent reflecting surface: Active or passive?" *IEEE Wireless Commun. Lett.*, vol. 10, no. 12, pp. 2659–2663, Dec. 2021.
- [10] Y. Han, S. Zhang, L. Duan, and R. Zhang, "Double-IRS aided MIMO communication under LoS channels: Capacity maximization and scaling," *IEEE Trans. Commun.*, vol. 70, no. 4, pp. 2820–2837, Apr. 2022.
- [11] X. Li, C. You, Z. Kang, Y. Zhang and B. Zheng, "Double-active-IRS aided wireless communication with total amplification power constraint," *IEEE Commun. Lett.*, vol. 27, no. 10, pp. 2817–2821, Oct. 2023.
- [12] M. Fu and R. Zhang, "Active and passive IRS jointly aided communication: Deployment design and achievable rate," *IEEE Wireless Commun. Lett.*, vol. 12, no. 2, pp. 302–306, Feb. 2023.